LETTERS
PUBLISHED ONLINE: 22 MAY 2011 | DOI: 10.1038/NPHOTON.2011.57

nature photonics

Active spatial control of plasmonic fields

Bergin Gjonaj[1]*, Jochen Aulbach[1], Patrick M. Johnson[1], Allard P. Mosk[2], L. Kuipers[1] and Ad Lagendijk[1]

The field of plasmonics[1] offers a route to control light fields with metallic nanostructures through the excitation of surface plasmon polaritons[2]. These surface waves, bound to a metal dielectric interface, can tightly confine electromagnetic energy[3]. Active control over surface plasmon polaritons has potential for applications in sensing[4], photovoltaics[5], quantum communication[6,7], nanocircuitry[8,9], metamaterials[10,11] and super-resolution microscopy[12]. We achieve here active control of plasmonic fields using a digital spatial light modulator. Optimizing the plasmonic phases through feedback, we focus surface plasmon polaritons at a freely prechosen point on the surface of a nanohole array. Digital addressing and scanning of surface plasmon polaritons without mechanical motion may enable novel interdisciplinary applications of advanced plasmonic devices in cell microscopy, optical data storage and sensing.

Positioning and focusing waves in transparent media requires fine tuning of the phase profile so that waves converge and constructively interfere at a point. A conventional lens uses refraction to redirect the waves to the focus and a well-designed lens shape to align the phase vectors of these waves. Owing to the fixed geometric shape of the lens, the position of the focus can only be controlled by mechanically moving the lens or changing the angle of incidence of the incident beam. Focusing and controlling the position where waves constructively interfere in complex structures requires new methods that are more versatile. Such methods have already been established for acoustics and microwaves in the context of time reversal[13]. Optical wavefront shaping has become a popular method that allows one to focus light even inside completely disordered materials[14,15].

Positioning and focusing surface plasmon polariton (SPP) waves in a controlled way is important for nanophotonic applications. To date, plasmonics offers only a limited flexibility in the control of light fields. As with the conventional lens the geometry is typically fixed, so for a given optical frequency the locations of optical field enhancement are also fixed. Recently, some breakthroughs have been made regarding active control, in which the intensity of the light fields is influenced in time, either through pump–probe[16–19] or coherent control[20]. Only in specific cases does this control also lead to spatial selectivity[21–23]. However, in these experiments the spatial selectivity is limited to a few modes predefined by the sample structure.

We demonstrate here a new level of control of SPP wavefronts. This control allows us to tune any SPP interference phenomenon with significant flexibility. Specifically, we show that we can generate and focus SPPs and scan the focus on a nanohole array with an electronically controlled spatial light modulator (SLM) and a standard helium neon laser. Because the light-to-SPP conversion process is coherent, the structured optical wavefront is projected onto the SPP wavefront. This conversion gives us full phase control of the SPPs, allowing us to shape the SPP wavefronts digitally. Because we use optimization loops to determine the necessary wavefront, our method is applicable to any plasmonic structure. Such flexible and digital control of SPPs is a large step towards interdisciplinary applications of advanced plasmonics.

The sample is a metallic nanohole array with a rich electromagnetic behaviour[24]. Subwavelength gratings offer potential for super-resolution either for dielectric[25] or metal–dielectric[26] configuration. Our sample is composed of a 200 nm gold film deposited on a 1 mm BK7 glass substrate. The array covers an area of $30 \times 30\ \mu\text{m}^2$ and the hole period (a_0) is 450 nm. Square holes were milled (focused ion beam) with sides of 177 nm. The SPP wavelength at the gold–air interface from incident radiation $\lambda_0 = 633$ nm is given by

$$\lambda_S = \lambda_0 \mathrm{Re}\sqrt{\frac{\varepsilon_m + \varepsilon_d}{\varepsilon_m \varepsilon_d}} \qquad (1)$$

where ε_m and ε_d are the dielectric constants of gold and air, respectively. Using tabulated bulk values for ε_m (ref. 27) we found that $\lambda_S = 600$ nm.

Our aim is to digitally control the amplitude and phase of SPPs locally on the surface of the sample. This control is achieved by imaging an SLM onto the surface of the sample, thus mapping each unit cell (pixel) of the SLM to a corresponding area on the sample. Amplitude and phase control of the SLM is achieved by grouping pixels into superpixels (see Supplementary Information). We independently control the amplitude and phase of 32×32 superpixels. The image of each superpixel locally excites surface waves[28] (to which SPPs are the dominant contribution).

A diagram of the 'set-up' is given in Fig. 1. On the basis of SPP momentum conservation, we designed the imaging system so that plasmons are launched towards the centre (Methods). The light reflected from the sample is imaged on the detector. This light includes both the direct reflection of the illuminating beam and the scattered light from SPPs. Because SPPs and reflected photons both contribute to the signal, it is important to separate their effects.

We achieve controlled launching and propagation of SPPs by spatially designing the amplitude of the incident light. The chosen amplitude profile, consisting of four bright ('on') SPP launching platforms and one central dark ('off') arena, fully separates plasmonic from optical effects and in addition is the necessary starting point for later focusing and scanning experiments. Any intensity detected inside the arena is purely plasmonic.

The resulting illuminated areas on a bare gold substrate are visible in Fig. 2a. The overall phase is constant. Each 'on' block is 10×8 superpixels in size. Because no SPPs are launched on bare gold owing to momentum mismatch, the image of Fig. 2a is used as a background reference and measure of contrast ratio between the 'on' and 'off' areas. The observed contrast is nearly three orders of magnitude, confirming that no photons enter the SPP arena.

[1]FOM-Institute for Atomic and Molecular Physics AMOLF, Science Park 104, 1098 XG Amsterdam, The Netherlands, [2]Complex Photonic Systems, Faculty of Science and Technology, and MESA+ Institute for Nanotechnology, University of Twente, PO Box 217, 7500 AE Enschede, The Netherlands.
*e-mail: b.gjonaj@amolf.nl

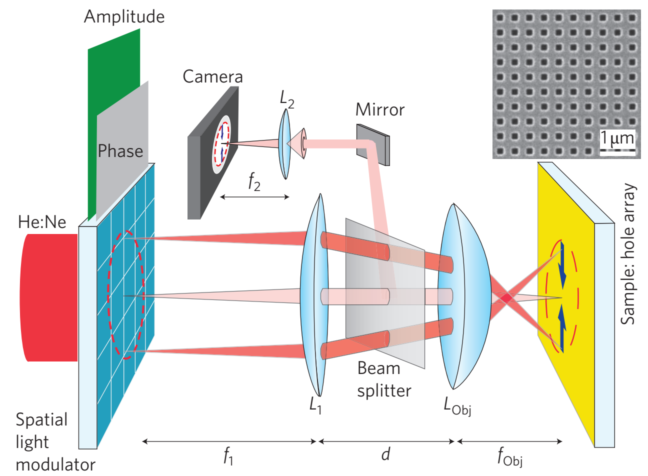

Figure 1 | Experimental 'set-up'. The SLM is projected onto the sample through the two-lens imaging system, L_1 and L_{Obj}. Demagnification is ×650. One pixel is imaged to nearly one diffraction-limit area. Every image point on the sample is formed with a different average angle of incidence (shown for three pixels). The amplitude and phase of each pixel of the SLM are independently controlled with a computer. The sample is a nanohole grating engraved on a gold film. The blue arrows illustrate the propagation of SPPs launched from two pixels of the SLM. The amplitudes and phases of the SPPs are effectively clamped to those of the launching pixels. The surface of the sample is imaged onto the camera through L_{Obj} and L_2.

When the designed amplitude profile is projected onto the hole array, SPPs propagate into the central dark arena. The nanohole array has a dual role: it is used to launch SPPs (bright rectangles in Fig. 2b–d) and to visualize the launched SPPs through their out-of-plane scattering in the central arena. SPPs are launched only along the direction of incident polarization as seen in Fig. 2c and d, consistent with expectations[29]. In Fig. 2b, the sample is illuminated both by the structured amplitude profile and by an additional white light source, showing both the hole array grating itself (fast amplitude modulation) and the laser light. This figure also demonstrates the optical resolution of the 'set-up'—sufficient to resolve the presence of the hole array pattern but not the shape of holes.

When two counterpropagating SPP waves interfere, a standing wave pattern of intensity is created. The observed period of the fringe pattern is clearly not half the SPP wavelength, as is expected for SPPs propagating on an ideally smooth and non-corrugated sample. The fringe period measured from Fourier analysis is 1 ± 0.05 µm. We attribute the fringe patterns to a Moiré effect between the true standing SPP wave and the periodicity of the arrays.

Now we present experiments of SPP focusing with digital phase control. The achieved SPP focusing is shown in Fig. 3. We use a phase optimization loop to focus SPPs at a pre-chosen target. This loop yields the optimal phase $\tilde{\phi}$ for each superpixel as well as the relative contribution C to focus. The amplitude profile is the same as for the bare gold case, with four launching areas and a central dark arena where only SPPs can propagate. The incident polarization is diagonal in relation to the grating lines so as to have all available angles (2π range) contributing to the focus, thereby maximizing the numerical aperture and resolution.

Successful focusing at the centre of the SPP arena is shown in Fig. 3a. The structured SPP wavefront produces an intensity in the designated target that is at least 20 times higher than the average SPP background of an unstructured wavefront. The measured size of the plasmonic focus is 420 nm, consistent with the diffraction limit of our optics. The flexibility of the method (scanning the focus) is demonstrated in Fig. 3b and c, which shows the SPP focus relocated without mechanical motion to controlled positions in the plasmonic arena. Thus the plasmonic arena is our field-of-view.

We interpret SPP focusing in terms of Green's functions connecting the electric fields at any two points. We idealize every 'on' superpixel n with a light source positioned at $\mathbf{r}_n$ and with phase $\phi(\mathbf{r}_n)$ and strength $A(\mathbf{r}_n) = 1$. The amplitude of the electric field (normalized to the incident field) at the target $\mathbf{r}_0$ due to these sources is

$$E\left(\mathbf{r}_0, \{\phi(\mathbf{r}_n)\}\right) = \sum_{n}^{N} g\left(\mathbf{r}_0, \mathbf{r}_n\right) \exp\left[i\phi(\mathbf{r}_n)\right] \qquad (2)$$

where $g(\mathbf{r}_0, \mathbf{r}_n)$ is the Green's function connecting each source to the target, and the sum runs over all the 'on' superpixels of the amplitude profile. The target field is maximal when all source contributions are in phase. The optimal phase for superpixel n is $\tilde{\phi}(\mathbf{r}_n, \mathbf{r}_0) = -\arg[g(\mathbf{r}_0, \mathbf{r}_n)]$. Imposing this phase to the superpixel yields an intensity increase of $C(\mathbf{r}_n, \mathbf{r}_0) = |g(\mathbf{r}_0, \mathbf{r}_n)|$. We can write

$$g\left(\mathbf{r}_n, \mathbf{r}_0\right) = C(\mathbf{r}_n, \mathbf{r}_0) \exp\left[i\tilde{\phi}(\mathbf{r}_n, \mathbf{r}_0)\right] \qquad (3)$$

Equation (3) implies that the recorded optimal phases and relative contributions of the superpixels give the Green's function for a plasmonic source located at that exact focus point. Thus the superpixels of the SLM effectively behave as amplitude- and phase-sensitive detectors. These results are valid for any Green's function or nanostructure and can be extended to the time domain[13] and the transmission matrix approach[30].

We demonstrate the first plasmonic system that operates as a 'black-box', requiring the user only to input the desired location of the nanoscale plasmonic focus that is the system's output. Specifically, we focus SPPs on hole arrays and locally scan the

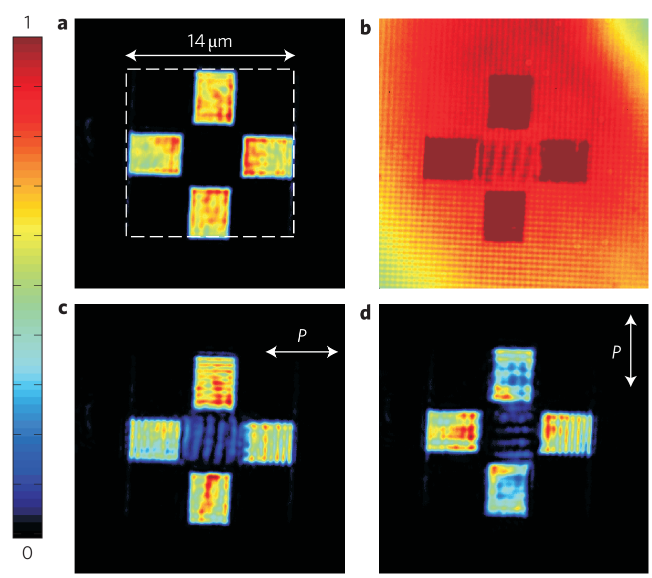

Figure 2 | Amplitude projection for uniform phase profile. In each image, bright rectangles are illuminated (amplitude = 1) SPP launching areas. SPPs are observed in the dark (amplitude = 0) central SPP arena. **a**, Bare gold reference (no SPPs launched). Dashed lines demarcate the SLM area. **b**–**d**, SLM projected on the 450 nm hole array: SLM image plus white light illumination to observe the hole array (**b**); SPPs launched toward the central SPP arena (**c**); vertical polarization (*P* in the figure) of incident light. The polarization is horizontal for the other images.

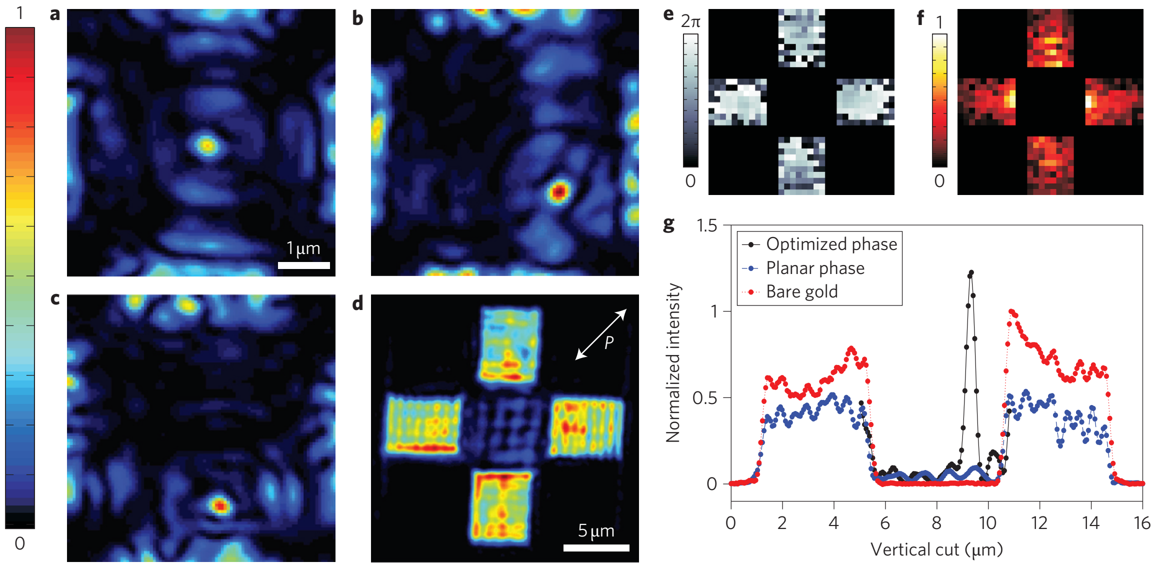

Figure 3 | Dynamic focusing of SPPs. **a**, Relative phases of the superpixels are optimized to focus SPPs at the centre of the SPP arena. The intensity in the target spot is purely plasmonic and 20 times higher than the average background of an unstructured plasmonic wavefront. The focus size is diffraction limited by the detecting optics. **b**,**c**, Demonstration of SPP focusing on freely chosen targets in the SPP arena. **d**, Background reference of an unstructured SPP wavefront (uniform phase profile). **e**,**f**, In achieving the focus of image **a**, we recorded the map of optimal phases (**e**) and of relative contributions (**f**) of the superpixels. Owing to reciprocity, these maps coincide with the phase and amplitude Green's function of an SPP source at the target. The amplitude map shows the decaying nature of SPPs. **g**, Quantitative analysis of SPP focusing showing vertical cuts of **b** and **d**. These cuts are normalized to the peak intensity of the bare gold case, also included in the graph.

focus freely over a field-of-view (SPP arena) without any mechanical translation. In achieving such dynamic focusing, we recorded amplitude and phase Green's functions. These digital records, which contain the full complexity of the Green's function, are used as self-calibrated inputs.

This digital plasmonic workbench is anticipated to enable interdisciplinary applications in microscopy, optical data storage and biosensing. Optimizing the chemical composition and nanostructure of the SPP arena enables confinement and manipulation of the achieved focus beyond the diffraction limit. Such a challenge requires near-field calibration and precise interpolation algorithms for scanning the focus in sub-100-nm steps.

Methods

Role of the oblique illumination scheme. In this section we describe the launching of SPPs. The SPP launching process on a regular hole array is a rich phenomenon in which momentum conservation plays a crucial role. The SPP momentum $2\pi/\lambda_S$ is the vector sum of the momentum produced by the grating orders of the hole array $(m, n)2\pi/a_0$ and the in-plane (interface) momentum component of incident light $k_0 \sin\theta$. For our sample, $a_0 < \lambda_S$; therefore, the magnitude of the hole array momentum is larger than the SPP momentum for any order. To satisfy SPP momentum conservation, the hole array momentum contributed to the SPP must be of opposite sign to the in-plane light momentum. As a consequence, the SPP travels in the direction opposite to the in-plane component of impinging light. In our experimental configuration, superpixels of opposing bright areas (amplitude = 1) are formed with opposing angles (θ and $-\theta$). This results in the launching of two counterpropagating waves and the formation of the standing fringe pattern. The slight bending (distortion) of the fringes (Fig. 2b) is due to a phase gradient from the surface curvature of the SLM. The bending can be easily compensated by loading an appropriate phase deviation to the planar wavefront.

Received 21 November 2010; accepted 1 April 2010;
published online 22 May 2011

References

1. Barnes, W. L., Dereux, A. & Ebbesen, T. W. Surface plasmon subwavelength optics. *Nature* **424,** 824–830 (2003).
2. Polman, A. Applied physics: plasmonics applied. *Science* **322,** 5903, 868–869 (2008).
3. Schuller, J. A. *et al.* Plasmonics for extreme light concentration and manipulation. *Nature Mater.* **9,** 193–204 (2010).
4. Prodan, E., Radloff, C., Halas, N. J. & Nordlander, P. A hybridization model for the plasmon response of complex nanostructures. *Science* **302,** 419–422 (2003).
5. Atwater, H. A. & Polman, A. Plasmonics for improved photovoltaic devices. *Nature Mater.* **9,** 205–213 (2010).
6. Altewischer, E., van Exter, M. P. & Woerdman, J. P. Plasmon-assisted transmission of entangled photons. *Nature* **418,** 304–306 (2002).
7. Akimov, A. V. *et al.* Generation of single optical plasmons in metallic nanowires coupled to quantum dots. *Nature* **450,** 402–406 (2007).
8. Ebbesen, T. W., Genet, C. & Bozhevolnyi, S. I. Surface-plasmon circuitry. *Phys. Today* **61,** 44–50 (2008).
9. Engheta, N. Circuits with light at nanoscales: optical nanocircuits inspired by metamaterials. *Science* **317,** 1698–1702 (2007).
10. Liu, N. *et al.* Plasmonic analogue of electromagnetically induced transparency at the Drude damping limit. *Nature Mater.* **8,** 758–762 (2009).
11. Ergin, T., Stenger, N., Brenner, P., Pendry, J. B. & Wegener, M. Three-dimensional invisibility cloak at optical wavelengths. *Science* **328,** 337–339 (2010).
12. Fang, N., Lee, H., Sun, C. & Zhang, X. Sub-diffraction-limited optical imaging with a silver superlens. *Science* **308,** 534–537 (2005).
13. Derode, A., Roux, P. & Fink, M. Robust acoustic time reversal with high-order multiple scattering. *Phys. Rev. Lett.* **75,** 4206–4209 (1995).
14. Vellekoop, I. M., van Putten, E. G., Lagendijk, A. & Mosk, A. P. Demixing light paths inside disordered metamaterials. *Opt. Express* **16,** 67–80 (2008).
15. Cizmar, T., Mazilu, M. & Dholakia, K. In situ wavefront correction and its application to micromanipulation. *Nature Photon.* **4,** 388–394 (2010).
16. Dionne, J. A., Diest, K., Sweatlock, L. A. & Atwater, H. A. PlasMOStor: a metal-oxide-Si field effect plasmonic modulator. *Nano Lett.* **9,** 897–902 (2009).
17. MacDonald, K. F., Samson, Z. L., Stockman, M. I. & Zheludev, N. I. Ultrafast active plasmonics. *Nature Photon.* **3,** 55–58 (2009).
18. Utikal, T., Stockman, M. I., Heberle, A. P., Lippitz, M. & Giessen, H. All-optical control of the ultrafast dynamics of a hybrid plasmonic system. *Phys. Rev. Lett.* **104,** 113903 (2010).
19. Temnov, V. V. *et al.* Active magneto-plasmonics in hybrid metal-ferromagnet structures. *Nature Photon.* **4,** 107–111 (2010).
20. Durach, M., Rusina, A., Stockman, M. I. & Nelson, K. Toward full spatiotemporal control on the nanoscale. *Nano Lett.* **7,** 3145–3149 (2007).
21. Aeschlimann, M. *et al.* Adaptive subwavelength control of nano-optical fields. *Nature* **446,** 301–304 (2007).
22. Li, X. & Stockman, M. I. Highly efficient spatiotemporal coherent control in nanoplasmonics on a nanometer-femtosecond scale by time reversal. *Phys. Rev. B* **77,** 195109 (2008).
23. Volpe, G., Cherukulappurath, S., Parramon, R. J., Molina-Terriza, G. & Quidant, R. Controlling the optical near field of nanoantennas with spatial phase-shaped beams. *Nano Lett.* **9,** 3608–3611 (2009).

24. Garcia-Vidal, F. J., Martin-Moreno, L., Ebbesen, T. W. & Kuipers, L. Light passing through subwavelength apertures. *Rev. Mod. Phys.* **82,** 729–787 (2010).
25. Sentenac, A. & Chaumet, P. C. Subdiffraction light focusing on a grating substrate. *Phys. Rev. Lett.* **101,** 013901 (2008).
26. Bartal, G., Lerosey, G. & Zhang, X. Subwavelength dynamic focusing in plasmonic nanostructures using time reversal. *Phys. Rev. B*, **79,** 201103 (2009).
27. Johnson, P. B. & Christy, R. W. Optical constants of the noble metals. *Phys. Rev. B* **6,** 4370–4379 (1972).
28. Lalanne, P. & Hugonin, J. P. Interaction between optical nano-objects at metallo-dielectric interfaces. *Nature Phys.* **2,** 551–556 (2006).
29. Devaux, E., Ebbesen, T. W., Weeber, J. C. & Dereux, A. Launching and decoupling surface plasmons via micro gratings. *Appl. Phys. Lett.*, **83,** 4936–4938 (2003).
30. Popoff, S. M. *et al.* Measuring the transmission matrix in optics: an approach to the study and control of light propagation in disordered media. *Phys. Rev. Lett.* **104,** 100601 (2010).

Acknowledgements

The authors thank E. van Putten and J. Cesario for stimulating and helpful discussions, and H. Zeijlermaker for sample fabrication. This work is part of the research programme of the 'Stichting voor Fundamenteel Onderzoek der Materie', which is financially supported by the Nederlandse Organisatie voor Wetenschappelijk Onderzoek.

Author contributions

B.G. was the primary researcher on this project, developing and building the set-up, carrying out all experiments and analysis, and writing the paper. All authors made essential contributions to the project and take full responsibility for the results presented.

Additional information

The authors declare no competing financial interests. Supplementary information accompanies this paper at www.nature.com/naturephotonics. Reprints and permission information is available online at http://www.nature.com/reprints/. Correspondence and requests for materials should be addressed to B.G.